

Host Galaxy Extinction, Observational Selection, and Type Ia Supernovae

E.D. Commins, R. Vogel, G. Aldering, and S. Perlmutter
Lawrence Berkeley National Laboratory
and Physics Department, University of California
Berkeley, California 94720

March 22, 2004

ABSTRACT

We develop models for extinction of Type Ia supernova light due to dust in spiral and spheroidal host galaxies. The models are based on well-known facts and concepts concerning galaxy morphology, star distributions, dust, and observational selection. Predictions of the models are compared with supernova data at low and high red shift. Our main conclusion is that at the present level of precision, host galaxy extinction is not a major source of systematic error in the determination of dark energy parameters.

1 Introduction

Type Ia supernovae, a relatively homogeneous class of very bright objects, have been employed with impressive success in the last few years as distance markers in cosmological investigations. Observations of scores of SNe Ia at high redshift ($z > 0.17$) have been achieved by two independent groups: the Supernova Cosmology Project (Perlmutter99, Knop03) hereafter referred to as SCP, and the High- z research team (Riess98, Tonry03). Both groups found that the SNe Ia are somewhat dimmer than would be expected according to the magnitude-redshift relation for the Einstein- deSitter model, where $\Omega_m = 1.0, \Omega_\Lambda = 0.0$. When one combines these results with observations of the fluctuation spectrum of the cosmic microwave background (CMB), (deBernardis02, Spergel03) which yield the constraint $\Omega_k \equiv \Omega_m + \Omega_\Lambda = 1$, one is led to the conclusion that $\Omega_m \simeq 0.25, \Omega_\Lambda \simeq 0.75$, (Knop03). These values imply that in the present epoch, “dark energy”, manifested by non-zero Ω_Λ , is of comparable importance to dark matter plus baryonic matter in determining the course of the Hubble expansion, and that the expansion is accelerating.

This unanticipated and fundamental discovery obviously demands a very high standard of evidence for its acceptance, and careful investigation of systematic

effects is necessary. For example, one must determine whether extinction of supernova light by intervening dust in our Galaxy, in intergalactic space, and/or in supernova host galaxies could contribute at least in part to the observed dimming as a function of red shift.

Galactic extinction has been studied for many years and is relatively well understood (Schlegel98, Mathis90, Draine03). Corrections to the supernova data arising from Galactic extinction can be made with relatively high confidence, and it is thus very unlikely that Galactic extinction could cause a serious systematic error. Moreover, for Galactic extinction to weaken the case for cosmic acceleration it would have to cause a dimming effect that *increases* with redshift. However, extinction generally *decreases* as wavelength increases; hence a residual systematic error due to Galactic extinction would very likely only strengthen the case for cosmic acceleration.

Unfortunately we know very little about possible intergalactic dust. There are no incontrovertible observations confirming its existence; only upper limits on its average density exist. Aguirre (99a, 99b, 00) proposed that dimming of supernova light might be caused by intergalactic dust rather than by acceleration of the Hubble expansion. He suggested that a portion of the dust created in galaxies during intense periods of star formation in past epochs might have been driven out of these galaxies, possibly by radiation pressure. The grains with the largest opacities would be most susceptible to this pressure: these would be the long needle-like grains that have absorption coefficients relatively independent of wavelength (“gray” opacity). Such large grains would also be least susceptible to destruction by various mechanisms such as sputtering by ionized gas.

The data on one Ia supernova (1997ff) at $z=1.7$ appear to contradict the gray dust hypothesis and to be consistent with cosmic acceleration (Riess01). However the uncertainties here are quite large; also one cannot rule out the possibility that gravitational lensing is responsible for the anomalously large brightness of 1997ff (Mortsell01).

In principle, a constraint on intergalactic gray dust can be obtained from comparison between the diffuse far infra-red background and that due to faint discrete sources (Aguirre00), but the uncertainties here are also too large to rule out the gray dust hypothesis categorically. In principle, a useful constraint on intergalactic gray dust could also be furnished by observation of X-rays from a distant bright QSO (redshift $z=4.3$), (Paerels02). If there were intergalactic gray dust in sufficient quantities to compromise the Ia supernovae results, scattering by this dust might result in a significant halo with a diameter ~ 1 arcmin surrounding the central X ray image. In fact, observations of the QSO point spread function yield no measureable halo, but uncertainties in dust grain size, shape and spatial distribution make it difficult to translate this result into a useful upper limit on extinction due to intergalactic gray dust (Windt02).

In this paper we concentrate on the problem of host galaxy dust. Our goal is to construct models of such dust simple enough to use and understand, but sophisticated enough to take into account the most important relevant observational facts concerning Sne Ia and their host galaxies. Work along these lines was already done by Hatano, Branch, and Deaton (Hatano98); here we try to

extend their efforts. In particular, we attempt to account for various observational selection effects that play a significant role in searches for high redshift SNe Ia. In Sec.2 of this paper, we summarize many of the relevant observational facts, in Sec.3 we describe the models for late type galaxies, and in Sec.4 we compare them with additional observations. Sec.5 is devoted to a spheroidal galaxy model and comparison with observations. Our conclusions are presented in Sec. 6.

2 The underlying observational facts.

2.1 Properties of dust.

Galactic dust is mainly confined to the Galactic plane, and its total mass is roughly 1% of the mass of interstellar gas. It consists of sub-micron sized particles, mainly graphite (and/or other forms of carbon such as nanotubes, buckyballs, etc.), silicates, polycyclic aromatic hydrocarbons (PAHs), some iron, and some ices (NH_3 , H_2O). Dust plays an important role in the energy balance of the Galaxy because it absorbs starlight (mainly in the UV and visible) and re-radiates it in the far infra-red (FIR). Perhaps 30% of the total luminosity of the Galaxy is due to this re-radiation. The opacity of dust is generally a decreasing function of wavelength; thus dust causes reddening of transmitted starlight.

Dust grains are probably formed in the outer envelopes of red giant stars and/or horizontal branch stars, as these stars suffer mass loss (Willson00); dust is also formed in supernova explosions. A typical grain is exposed to many physical processes and undergoes radical transformations during its finite lifetime (Salpeter77). Grain-grain collisions can cause grains to be shattered, but in such collisions, grains can also stick together to form larger objects. Intense stellar radiation can evaporate volatile molecules from grain surfaces. UV can photo-ionize grains. Collisions with fast ions can sputter the grains (drive atoms from the grain surface). Shock waves from supernova remnants can fragment grains, and radiation pressure as well as gas-grain collisions can accelerate them. If grains are electrically charged, and a fraction undoubtedly are, then their motion is influenced by galactic magnetic fields. All in all, a typical grain is influenced by many forces, and has a very complex history.

Dust grains aid in star formation, facilitating the gravitational collapse of gas clouds by radiating away energy in the infra-red. Thus for various reasons the dustiest regions of a galaxy are the regions of most active star formation (i.e. spiral arms of spiral galaxies). In a previous epoch ($z \sim 0.5 - 1$) star formation was far more vigorous than it is now; hence we may assume that many galaxies in that epoch were dustier than they are now. Conversely, in elliptical galaxies where star formation ceased long ago, there is relatively little dust.

The absorption and reddening by dust, which vary from one line of sight to another, are characterized by the following quantities, defined separately for each species of dust grain (as categorized by composition, size, and shape):

- a) The opacity per gram of the i th component κ_i in cm^2/g ;

b) The mass density of the i 'th dust component: ρ_i in g/cm^3 .
 From these quantities we construct the total absorption coefficient:

$$\alpha(\lambda, \mathbf{r}) = \sum_i \rho_i(\mathbf{r}) \kappa_i(\lambda, \mathbf{r}) \quad (1)$$

The optical depth at wavelength λ from an observer at the origin to a distance R is:

$$\tau(\lambda) = \int_0^R \alpha(\lambda, \mathbf{r}) dr \quad (2)$$

The extinction, in magnitudes, is defined as:

$$A(\lambda) = 2.5 \log_{10}(e) \tau(\lambda) = 1.086 \tau(\lambda) \quad (3)$$

It is also convenient to define the selective extinction:

$$E(\lambda_1 - \lambda_2) = A(\lambda_1) - A(\lambda_2) \quad (4)$$

and the ratio of total to selective extinction:

$$R_V = \frac{A_V}{E(B - V)} \quad (5)$$

In Fig. 1 we plot A_λ/A_V versus $x \equiv \lambda^{-1}$ for 4 different values of R_V . The curves are drawn from analytical fits to large amounts of Galactic data, first constructed by Cardelli, Clayton and Mathis (Cardelli89, Fitzpatrick99). These fits are represented by the equation:

$$\frac{A_\lambda}{A_V} = a(x) + \frac{1}{R_V} b(x) \quad (6)$$

where $a(x)$, $b(x)$ are two purely formal analytic functions with no direct physical significance.

We note the following important points relevant to Fig.1. The value of R_V depends on the environment along the line of sight. A direction through low densities of the interstellar medium *usually* yields a low value: $R_V \simeq 2$, while lines of sight through dense clouds usually give $R_V \simeq 4 - 6$. A typical value for many observations in the Galaxy is $R_V = 3.1$. For low values of R_V , $\frac{A_\lambda}{A_V}$ varies strongly with x in the UV, while for larger values of R_V , the dependence of $\frac{A_\lambda}{A_V}$ on x in the UV is much weaker. This is probably due to the fact that in the interior of dense clouds, which are relatively well shielded from intense UV, various grain destruction mechanisms are diminished, and the growth of relatively large grains by coagulation is facilitated. (One may readily understand from the theory of scattering that large grains have opacities that vary more slowly with x than that of small grains). In the visible and especially in the IR, the dependence of $\frac{A_\lambda}{A_V}$ on R_V is not nearly as dramatic as in the UV, as can be seen by inspection of Fig. 1 in the range $x < 2.5 \mu^{-1}$.

The large bump in each curve of Fig.1 at $x = 4.6 \mu^{-1}$ ($\lambda = 217nm$) is probably

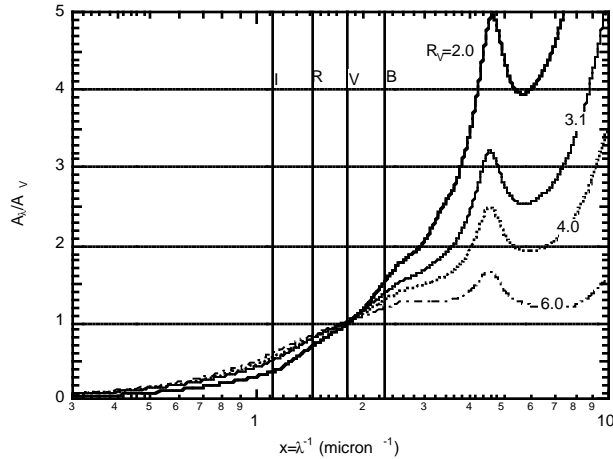


Figure 1: A_λ/A_V is plotted versus $x = \lambda^{-1}$ for 4 different values of R_V . The solid vertical lines indicate the nominal wavelengths of the standard photometric bands B, V, R, and I.

due to graphite and/or other forms of carbon that are spectroscopically similar (Draine03, Will99). Laboratory experiments show a resonance in graphite at this wavelength with the required oscillator strength and line-width.

Although it is not possible to see them in Fig.1, there are other significant resonances in the extinction curve (Draine03). For example, in the visible approximately 40 absorption bands exist, the strongest of which is at 443 nm. There are also strong emission bands in the NIR at 3.3, 6.2, 7.7, 8.6, and 11.3 μ . These wavelengths all correspond to C-H or C-C bond vibrations in aromatic hydrocarbons, which could occur as polycyclic aromatic hydrocarbons and/or as more complex aromatics. Bands at 9.7 and 18 μ are probably due to SiO_4 tetrahedra in more complex structures such as olivine: $(Mg, Fe)_2SiO_4$. A band at 3.1 μ is probably due to water ice or ammonia ice.

Roughly speaking, for a typical line of sight in our neighborhood of the Galaxy in B band (445 nm), $\alpha_B \approx 3 kpc^{-1}$, corresponding to an opacity $\kappa \approx 3 \cdot 10^4 cm^2 g^{-1}$. While there is no unique prescription for the grain size distributions and for the proportions of graphite, silicates, aromatic hydrocarbons, and ices that account for all the observations, there is general agreement on a “standard Galactic dust model”, first formulated by Mathis, Rumpl, and Nordsieck (Mathis77), developed by Draine and Lee (Draine84), and refined by Weingartner and Draine (Weingartner01, Draine03). According to this model, along a “typical” line of sight both graphite and silicate grains are distributed in size according to the formula:

$$dn_{grain} = C \cdot n_H a^{-3.5} da \quad (7)$$

where a is the grain radius (here, for simplicity the grains are assumed to be spherical); C is a constant: $C_{graphite} = 10^{-25.13} cm^{2.5}$, $C_{silicate} = 10^{-25.11} cm^{2.5}$,

n_H is the number density of hydrogen nuclei (in atoms or molecules), and $a_{min} \approx .005\mu$, $a_{max} \approx .25\mu$. This yields a dust mass density $\rho \approx 10^{-25}n_H gcm^{-3}$. Clearly the “standard” model assumes that the dust density is everywhere proportional to the hydrogen nuclear density, it ignores the spatial variations in size and composition that are well known to occur, and it also ignores the fact that many grains are not spherical, but rather elongated “needles” with large aspect ratios. The evidence for this is the well-known phenomenon of starlight polarization (Hall49, Hiltner49), probably caused at least in part by the alignment of elongated paramagnetic grains perpendicular to the Galactic magnetic field (Davis51, Draine03a). It is also known from various laboratory experiments and theoretical analyses that crystal growth from the vapor phase is strongly favored at “screw-dislocation sites”, and in this case long needle-like crystals tend to form (Frank49, Sears55, Bacon60, Donn63).

The properties of dust just briefly summarized were determined almost exclusively from observations confined to our local region of the Galaxy. How can we be confident that the dust in other galaxies has similar properties? Quantitative evidence concerning dust distributions in other spiral galaxies is obtained from a variety of sources, including IRAS surveys (Soifer87), ISO surveys (Genzel00), CCD photometry and modelling of nearly-edge-on spirals (Knapen91, Jansen94, Mathews01, Dalcanton02, Masters03), HST observations of spirals backlit by elliptical galaxies (Keel01) and gravitational lensing of quasar light by various galaxies (Falco99). The data strongly suggest that the basic physical processes governing the production and evolution of dust grains are the same as in our local region of the Galaxy, but specific environmental features, such as the relative numbers of graphite and silicate grains, may vary considerably from one locale to another. In the absence of more detailed and exact knowledge, one must characterize this variation by just three (related) parameters: the dust density and opacity, and R_V or its equivalent.

2.2 Classification of supernova-host-galaxy morphology.

Van den Bergh, Li, and Filippenko (van den Bergh02) classified the host galaxies of 177 low-z supernovae. For a tabulated subset of 148, 50 are Ia, 11 are Ia-pec, 19 are Ibc, 60 are II, and 8 are IIin. While the Ibc, II, and IIin (core collapse) supernovae occurred exclusively in late type galaxies (with one possible exception), the Ia and Ia-pec were found in galaxies of morphological types E to Sc. This result, in agreement with earlier findings (van den Bergh91), is consistent with the following picture: core collapse Snc progenitors are massive stars that evolved quickly and were thus born in regions of current star formation, i.e. the spiral arms of spiral galaxies. However, Type Ia progenitors are probably C/O white dwarfs that have reached the Chandrasekhar limit by accretion from a binary companion (Hillebrandt00 and references therein), and could thus have originated in a variety of stellar populations, young or old.

Ivanov, Hamuy, and Pinto (Ivanov00) gave the host galaxy classifications of 62 separate low-z Snc Ia previously discussed by Phillips et al (Phillips99).

Sullivan and Ellis (Sullivan03) classified the host galaxies of most of the high

redshift Sne Ia employed by SCP in Perlmutter99. In Table 1. we summarize these results. The Sne Ia are distributed in 3 broad categories of galaxies: E: (Spheroidal:E and S0); SI: (early spirals:Sa,Sab,Sb); and SII: (late spirals and irregulars:Sbc,...).

Table 1. Numbers of Sne Ia, Ia pec found in galaxies of various morphological types.

	E	SI	SII
(Ivanov00)	23	17	22
(van den Bergh02)	15	34	12
Total (low z)	38	51	34
(Sullivan03) (high z)	10	10	19

The data of Table 1 suggest that for low z , the frequency of Sne Ia from early spirals is slightly larger than for the other two categories; while for high- z , late spirals and irregulars dominate. This may be due at least partly to the fact that at large z ($z \approx 1$), the population of irregular galaxies (mainly blue dwarfs) relative to that of large spirals was considerably higher than it is today (Brinchmann98). Elliptical and S0 galaxies comprise $\approx 25 - 30\%$ of the hosts in each case.

2.3 Distribution of observed Sne Ia with respect to redshift and extinction.

Were it not for observational selection and possible evolutionary effects, one would expect that the number of Type Ia supernovae observed between redshifts z and $z+dz$ should be given by the following formula:

$$\frac{dN}{dz} = const \cdot \frac{1}{(1+z)\sqrt{1+\Omega_m(z^3+3z^2+3z)}} \left[\int_0^z \frac{dx}{\sqrt{1+\Omega_m(x^3+3x^2+3x)}} \right]^2 \quad (8)$$

where we assume that $\Omega_m + \Omega_\Lambda = 1$. In Fig. 2 we plot dN/dz versus z for $\Omega_m = 0.25, \Omega_\Lambda = 0.75$, and compare it to a sample of 40 detected Ia supernovae from spiral and irregular hosts (Perlmutter99, Sullivan03, Knop03), and 10 from spheroidal hosts (Perlmutter99, Sullivan03). Fig. 2 indicates that as z increases above $\approx .45$, the probability of observation of a supernova per unit z per unit time decreases for Sne in early-type hosts, and decreases quite sharply for late-type hosts.

This sharp decrease appears to be due at least in part to observational selection associated with extinction, arising from the relatively large amount of dust in spiral galaxy disks. For any assumed values of Ω_m and Ω_Λ the apparent magnitude m of a "standard" Type Ia supernova increases as z increases. However, given constant conditions of observation such as telescope and detector sensitivity, seeing, etc., there is a limiting red shift $z = z_0$ corresponding to a

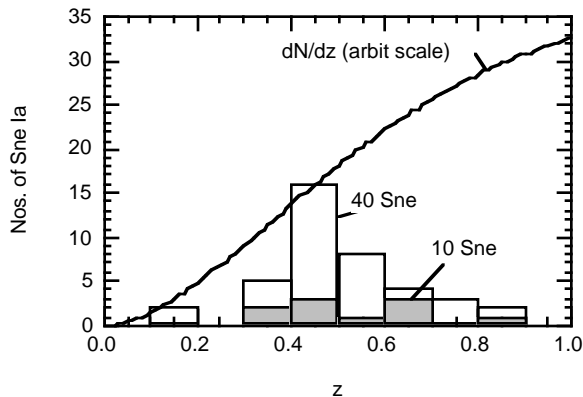


Figure 2: Comparison of dN/dz (arbitrary scale) with histograms of 40 Sne Ia from late-type hosts, and 10 Sne Ia from spheroidal hosts.

maximum apparent magnitude m_0 beyond which one cannot observe a Ia supernova reliably. (Although observation conditions were certainly not uniform for the supernovae of Fig. 2, $z_0 \approx 1.0 - 1.2$ is a reasonable approximation for the entire sample.) The decrease in probability of observation per unit z per unit time occurs because as z approaches z_0 from below, fewer and fewer supernovae have sufficiently small extinction so that $m < m_0$.

This point is elucidated, if only qualitatively, from inspection of Fig. 3, in which are collected the redshifts and rest frame V-band extinctions A_V of 92 high-redshift supernovae with $0.124 \leq z \leq 1.76$; (Tonry03, Sullivan03, Knop03).

Admittedly, the data of Fig. 3 are far from ideal: the host galaxies are of di-

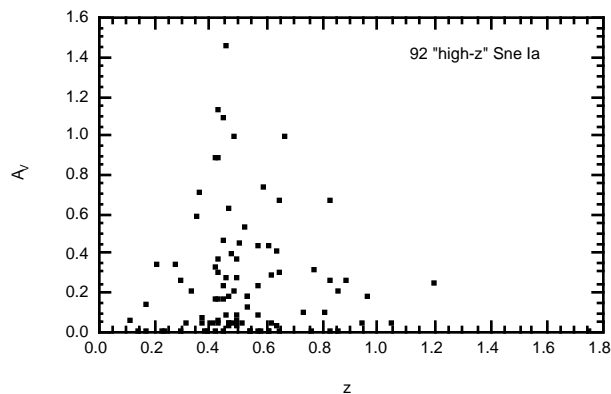


Figure 3: A_V plotted vs. z for 92 Sne Ia with $z > 0.12$. (Tonry03, Sullivan03, Knop03).

verse morphological types, in many cases the uncertainties in A_V are large, and observational conditions were certainly not uniform. Nevertheless, we can dis-

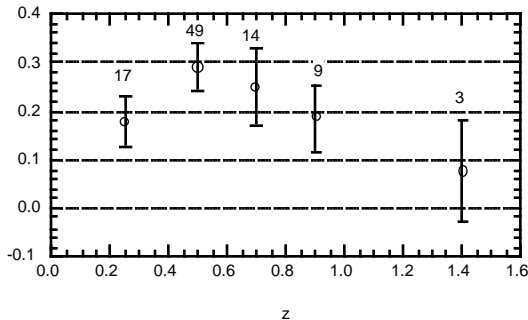


Figure 4: $\langle A_V \rangle$ vs z for data of Fig.3; z -bins .12-.4, .4-.6,.6-.8, .8-1.0,1.0-1.8.

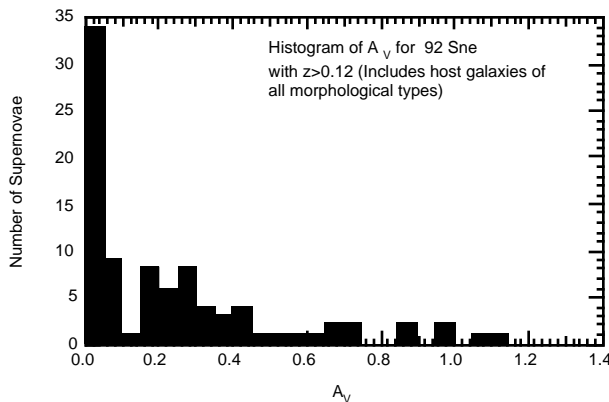


Figure 5: Data of Fig. 3.

cern a trend toward lower average extinctions as z increases above .45. This is also suggested in Fig.4, where we bin these supernovae according to redshift, and plot the average A_V and its uncertainty for each bin. In Fig. 4, the numbers above each error bar are the numbers of supernovae in each bin.

It is apparent from Fig.3 that at any given z there are relatively many supernovae with little or no extinction, in addition to a number with extinctions extending to large values. This may also be seen in Fig. 5, in which we bin the supernovae of Fig.3 with respect to A_V , regardless of z . It is easy to understand the distribution shown in Fig.5 in qualitative terms. Consider a disk-like host galaxy at some arbitrary inclination angle. The light from a supernova on the side of the galaxy nearest to the observer encounters little dust and suffers little or no extinction as it travels to the observer. Such a supernova will contribute to the large peak near $A_V = 0$. On the other hand if a supernova is buried deep in the interior of the disk, or is on the “far side”, it will have considerable extinction, and will contribute to the long tail in the distribution. As we shall see, all of the main features just described in connection with Figs. 2-5 are

revealed in the extinction models that we now present.

3 Spiral Galaxy Extinction Models

We wish to construct mathematical models of extinction in a typical spiral galaxy. For this we need a spatial distribution function for the dust absorption coefficient, and another distribution function for the Ia supernova progenitor stars. It is natural to start with our Galaxy, since measurements made with the COBE satellite provide sufficient information for construction of a detailed map of dust and stars in the Milky Way disk, by Drimmel and Spergel (Drimmel01). In the Drimmel-Spergel model, the inventory of stars consists of a bulge component, an axially symmetric disk, and spiral arms. The dust consists of an axially symmetric disk portion and a spiral arm portion. In our spiral galaxy model 1, we employ many of the Drimmel-Spergel features unmodified, but we do change a number of them for the sake of simplicity, and/or for a compelling physical reason. We now discuss each feature in turn.

3.1 Bulge stars

A spiral galaxy consists of a relatively thin disk and a central bulge, as well as an extended halo. Bulges are frequently not spherically symmetric, and can even be triaxial, but it is a reasonable first approximation to assume spherical symmetry. The surface brightness $I(r_B)$ of the typical bulge is then reasonably well described by the deVaucouleurs distribution (deVaucouleurs48, Binney98):

$$I = I_e \exp\{-7.67[(\frac{R}{R_e})^{.25} - 1]\} \quad (9)$$

where R, R_e are in plane polar coordinates, and R_e is the effective radius within which 1/2 of the surface luminosity is contained. A median value of R_e for a wide range of spirals is $R_e = 2.6 \text{ kpc}$ (Kent85, Simien86). According to Simien and deVaucouleurs (Simien86) there is no pronounced dependence of the median R_e on Hubble T type, except for a possible weak maximum at $T=1$, and a slight drop for $T > 6$.

It can be shown that the spherically symmetric luminosity density $j(r)$ is related to the surface brightness by the formula:

$$j(r) = -\frac{1}{\pi} \int_R^\infty \frac{\partial I}{\partial R} \frac{dR}{\sqrt{R^2 - r^2}} \quad (10)$$

where r is in spherical polar coordinates. The simple function:

$$j_B(r) = \frac{const}{(r^2 + a^2)^{3/2}} \quad (11)$$

where $a=0.7 \text{ kpc}$, is an adequate approximation for our purposes. Can we assume that the bulge luminosity density $j(r)$ faithfully describes the distribution

of Sne Ia progenitors in the bulge? This is plausible, since the bulge consists mainly of old stars, and as we have mentioned, Type Ia progenitors appear to be C/O white dwarfs driven to the Chandrasekhar limit by accretion from binary companions.

The relative importance of bulge and disk in a spiral galaxy can be characterized by the bulge-to-total luminosity ratio B/T. As is well known, B/T decreases steadily as one goes from early to late spiral types (Simien86). In the Drimmel-Spergel model, B/T=0.20. We have carried out Monte Carlo calculations of extinction for a variety of B/T values, ranging from 0 to 0.75.

3.2 Disk Stars: axially symmetric portion.

The radial brightness distribution of disk stars in a spiral galaxy is usually characterized by the function:

$$I_{disk}(r_0) = const \cdot exp\left(-\frac{r_0}{h_1}\right) \quad (12)$$

where r_0 is in cylindrical polar coordinates (Binney98). In the Drimmel-Spergel model, $h_1 = 2.26kpc$, and unless otherwise stated we adopt this value. Does the disk brightness function (12) correspond to the radial distribution of disk Sne Ia progenitors? This is not evident a priori, since disks often contain young stellar populations responsible for a large fraction of the disk luminosity, whereas, as previously stated, Sne Ia progenitors may be quite old. Nevertheless for lack of compelling evidence to the contrary, we shall assume that the two distributions are the same.

In a typical spiral galaxy, the disk stellar population z-distribution (where z is normal to the disk plane) can be modeled by the function $sech^2(z/h_z)$, where $h_z \approx .33 - 1kpc$ is the scale height (Binney98). In the Drimmel Spergel model, $h_z = .282$ kpc. However, the scale height of Sne Ia progenitors is very likely to be considerably greater. Observed white dwarfs (in our locale of the Galaxy) have scale heights of .4 to .6 kpc (Majewski02), and a study of vertical color gradients in late-type edge-on galaxies reveals the ubiquitous existence of low-luminosity, relatively dust-free thick disks containing old red stars (Dalcanton02). It is reasonable to assume that Sne Ia progenitors are to be found preferentially in this population. Thus we shall assume unless otherwise noted that the scale height for Sne Ia progenitors is $h_z = 0.5kpc$.

3.3 Disk stars- spiral arm portion.

The Drimmel-Spergel model contains a detailed description of the disk spiral arms. Since in our Monte Carlo calculations it is convenient to maintain axial symmetry, we replace the Drimmel-Spergel spiral arms by three concentric rings, with properties chosen to give an approximate match to the average properties of those spiral arms. Our rings are at disk radii 3.5, 5, and 7 kpc. Thus, in our model 1 the probability of locating a supernova progenitor between r_0 and

$r_0 + dr_0$, and between z_0 and $z_0 + dz_0$ in disk cylindrical polar coordinates, is proportional to:

$$df(r_0, z_0) = \exp\left(-\frac{r_0}{h_1}\right) \left[1 + \sum_{n=1}^3 a_n \exp(-[b_n(r_0 - c_n)]^2) \right] \cdot \text{sech}^2(z_0/h_z) \cdot r_0 dr_0 dz_0 \quad (13)$$

where the axially symmetric disk and the rings at 3.5, 5, and 7 kpc are represented by the first, second, third, and fourth terms respectively, all lengths are in kpc, and $a_1 = a_2 = 1.28$, $a_3 = 1.27$, $b_1 = 2.01$, $b_2 = 1.41$, $b_3 = 1.01$, $c_1 = 3.5$, $c_2 = 5.0$, and $c_3 = 7.0$.

3.4 Dust: axially symmetric and spiral arm portions.

As in the case of the stars, we replace the Drimmel-Spergel dust spiral arms by concentric rings at $r_0 = 3.5, 5.0$ and 7.0 kpc , but otherwise we choose the parameters to obtain the closest possible match to the Drimmel-Spergel B-band absorption coefficient α_B . Thus, we employ the following formula:

$$\alpha_B(\rho, z) = b \cdot g \cdot \left\{ 25.7 \exp\left(-\frac{\rho}{h_2}\right) \text{sech}^2\left(\frac{z}{h_D}\right) + \sum_{n=1}^3 u_n \exp(-v_n[\rho - c_n]^2) \exp(-[w_n z]^2) \right\} \text{kpc}^{-1} \quad (14)$$

Here, ρ and z are cylindrical polar coordinates of a dust element (in kpc), and the dust radial scale is h_2 , ($=2.26$ kpc unless otherwise noted). Also, b is an important overall absorption coefficient factor, which can be chosen at will: $b=1$ in the Drimmel-Spergel model but we have chosen b anywhere from 0.01 to 10 in various calculations. Also, g describes the well-known ‘‘hole’’ in the dust density near the disk origin:

$$g = \exp[-.25(\rho - 4)^2], \rho < 4 \text{ kpc} \\ g = 1, \rho \geq 4 \text{ kpc} \quad (15)$$

Furthermore h_D describes the dust vertical scale which includes the observed ‘‘flaring’’ of the dust distribution at large z : $h_D = .134$ kpc if $\rho < 4.4 \text{ kpc}$, while $h_D = .134 + .0148(\rho - 4.4) \text{ kpc}$ if $\rho \geq 4.4 \text{ kpc}$. Finally, $u_1 = 7.03$, $u_2 = 4.22$, $u_3 = 2.5$, $v_1 = 19.93$, $v_2 = 9.77$, $v_3 = 4.94$, $w_1 = w_2 = 12.5$ and $w_3 = 8.77$.

The parameters we have just described are designed to fit the Drimmel-Spergel model of the Galaxy rather closely, and they are therefore quite specialized. We have thus constructed a second and simpler model as well (Model 2). Here, we replace the factor g by unity to eliminate the dust ‘‘hole’’, and we also eliminate the rings that approximate the spiral arms for both dust and stars. Despite these simplifications, the results obtained with Model 2 are quite similar to those of Model 1, provided the same choices are made for h_1, h_2, h_z , and h_D . In Fig. 6, we plot α_B versus ρ for $b=1$ and $z=0$, to illustrate the distinction between Models 1 and 2.

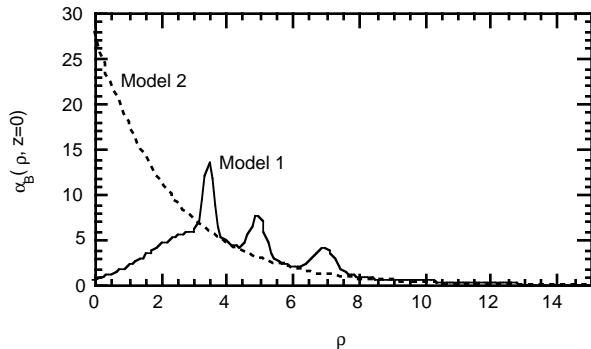


Figure 6: B-band absorption coefficient α_B plotted vs. ρ for $z=0$. Models 1,2

3.5 Spiral model geometry

Fig. 7 shows the geometry used for the axially symmetric models of spiral galaxy host extinction. We assume a galaxy with origin at O . Consider a plane parallel to the galactic plane, but displaced from it by a distance z_0 , ($OO' = z_0$). Let P be the location of the supernova in that plane, at radial distance r_0 from O' . Let $\mathbf{R} = PP'$ be a vector directed toward the observer, through a small element of dust at P' . \mathbf{R} is inclined by angle θ with respect to the normal to the galactic plane. Let the projection of \mathbf{R} in the plane be PQ . Construct the line segment AB through O' that is parallel to PQ . Then the plane polar coordinates ρ, z of the element of dust are given by:

$$\rho = \sqrt{R^2 \sin^2 \theta + r_0^2 - 2Rr_0 \sin \theta \cos \beta} \quad (16)$$

and

$$z = z_0 + R \cos \theta \quad (17)$$

Given the location of the supernova at $P = (r_0, \beta, z_0)$, the inclination angle θ , (both chosen by the Monte Carlo method) and the absorption coefficient α_B as a function of ρ, z , we can calculate the extinction:

$$A_B = 1.086 \int_0^\infty \alpha_B(\rho, z) dR \quad (18)$$

by numerical integration. The supernova bulge and disk distributions are given by (11, 13) respectively, and as previously stated B/T can be chosen at will; values range from 0.0 to 0.75.

So far we have assumed that all of the dust in a spiral galaxy originates in the disk, but one may properly ask whether the bulge might also contain dust. After all, bulges in spiral galaxies are similar to elliptical galaxies, and the latter do have some dust. In fact we have extended the model just described to include this possibility, but we find that the resulting changes in numerical results are

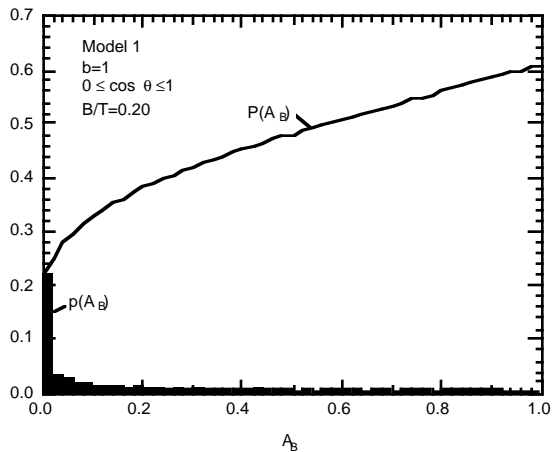


Figure 8: The probability distribution $p(A_B)$ and the cumulative probability distribution $P(A_B)$ plotted vs. A_B for the conditions indicated.

centile: $A(.8)$ such that $P[A(.8)]=.8$. For the conditions of Fig. 8, $A(.5)=.58$ and $A(.8)=2.3$. Note also that since the absorption coefficient α_B is proportional to b , so also are $\langle A \rangle$, $A(.5)$, and $A(.8)$ proportional to b .

Fig. 9 shows how $A(.5)$ depends on the inclination angle θ and on the relative number B/T of supernovae in the bulge, for $b=1$. The results are seen to depend

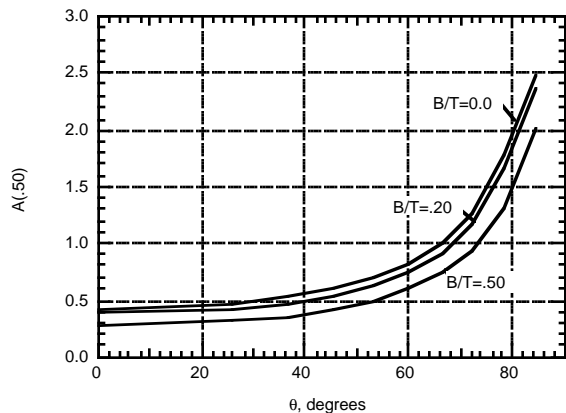


Figure 9: $A(.5)$ plotted vs. θ for $b=1$ and $B/T=0, .20,$ and $.50$. Model 1.

only weakly on B/T . The dependence on θ is also weak for $0 \leq \theta \leq 45^\circ$; but then $A(.5)$ increases rapidly for angles approaching 90° . This has obvious implications for observational bias against detecting supernovae in edge-on galaxies. Fig. 10 illustrates the effect of observational selection on the detection of supernovae close to the center of a spiral galaxy. Here we employ Model 2. Separate

histograms show the probabilities to observe a supernova in annular rings between r_0 and $r_0 + 1$ kpc regardless of extinction; and the same probabilities for all supernovae with extinction $A_B \leq 0.5$. Obviously the ratio of the latter to the former probability decreases as one goes closer to the origin. Somewhat similar results are obtained for Model 1, and a similar result would be obtained for calculation of the radial dependence of galactic starlight itself, except that here it would be necessary to take into account the significant effects of scattering as well as absorption, by employing a proper radiative transport calculation.

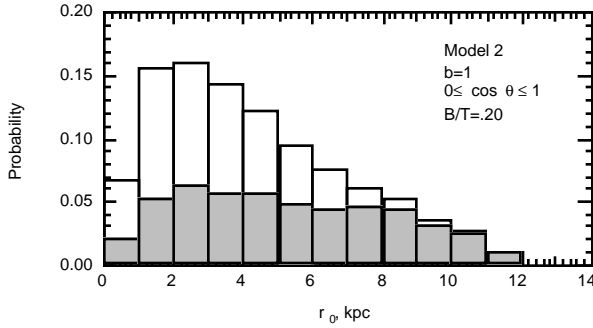


Figure 10: Observation probabilities vs. radial distance from center. White histogram: all supernovae regardless of extinction; shaded histogram: supernovae with $A_B \leq 0.5$.

Fig. 11 illustrates the dependence of $p(A)$ on the supernova progenitor scale height h_z . As expected, a reduction in h_z causes a decrease in the peak of $p(A)$ near $A \approx 0$, and an increase in the tail of the distribution for large values of A .

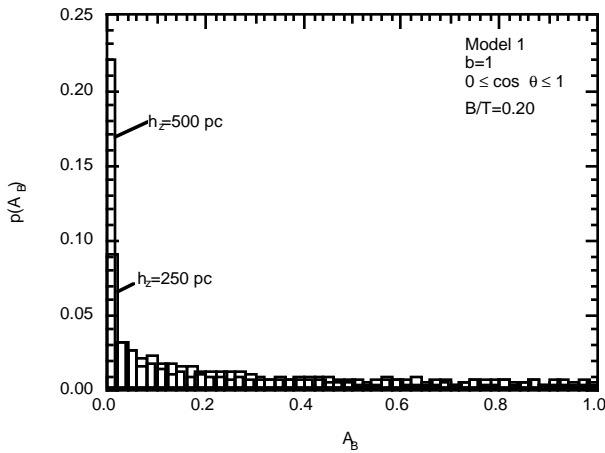


Figure 11: Dependence of $p(A_B)$ on the supernova progenitor scale height h_z .

We can simulate the effect of dust clumping by varying b randomly about a predetermined average value as we integrate the absorption coefficient along the line of sight; (recall eq'n 18). The length scale of this variation can also be chosen at will in the Monte Carlo calculation. Fig. 12 shows the results obtained when this length scale is 1 kpc, and the distribution function for b is exponential, with mean value unity. As one might expect intuitively, clumping causes $P(A_B)$ to increase somewhat for small values of A_B ; but for large values of A_B , $P(A_B)$ is slightly lower than for the case of no clumping. When the clumping length scale is much less than 1 kpc, the effect of clumping is much less noticeable.

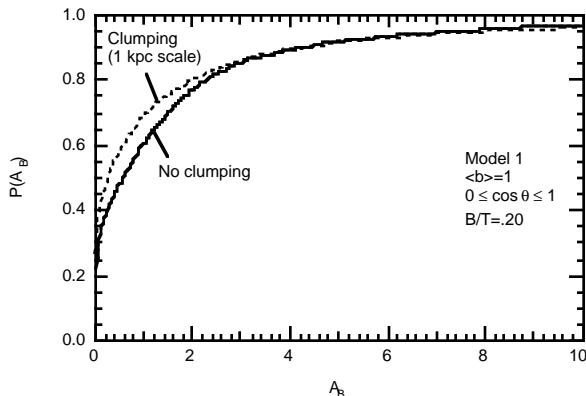


Figure 12: The effect of clumping is illustrated by comparison of the two curves.

We next consider a very important observational selection effect already mentioned in Sec.2, in connection with Figs 2,3, and 4. As we stated, for any assumed values of Ω_m and Ω_Λ the apparent magnitude m of a “standard” Type Ia supernova increases as z increases. Now, given constant conditions of observation such as telescope and detector sensitivity, seeing, etc., there is a limiting red shift $z = z_0$ corresponding to a maximum apparent magnitude m_0 beyond which one cannot observe a SN1a reliably. For example, for the proposed space observatory SNAP, $z_0 \approx 2$. The observational selection effect we refer to arises because as z approaches z_0 from below, less and less extinction from host galaxy dust can be tolerated before we reach m_0 . In what follows we shall call this the “cutoff” effect.

To put it on a quantitative basis, we recall the magnitude red-shift relation, derived from Friedmann’s equation (Carroll92). Assuming that $\Omega_m + \Omega_\Lambda = 1$ this may be written:

$$m = M + C + 5 \log_{10} \left[(1+z) \int_0^z \frac{dx}{\sqrt{1+x(x^2+3x+3)\Omega_m}} \right] \quad (19)$$

where M is the absolute magnitude of a standard SN1a and C is a constant. (Here, for simplicity, we ignore the small intrinsic variation in M from one

supernova to another). Now, let A_0 be the limiting extinction which at $z < z_0$ increases the magnitude m to m_0 :

$$A_0 = m_0 - m \quad (20)$$

Then from (19) we obtain:

$$A_0 = 5 \log_{10} \left[\frac{(1+z_0) \int_0^{z_0} \frac{dx}{\sqrt{1+\Omega_m(x^3+3x^2+3x)}}}{(1+z) \int_0^z \frac{dx}{\sqrt{1+\Omega_m(x^3+3x^2+3x)}}} \right] \quad (21)$$

Numerical evaluation of (21) for $z_0=1.0$, for example, reveals that to a good approximation:

$$A_0(\Omega_m = 0.25, \Omega_\Lambda = 0.75) = 2.5 \ln\left(\frac{1.0}{z}\right) \quad (22)$$

where (22) is a valid approximation for $z > 0.15$.

In Fig. 13 we plot the median extinction $A(.5)$ of all supernovae with extinction less than $A_0(z)$, as a function of z , for $b=.1, .2, .4, .8, 1.6, 3.2$, and 6.4 , and for $z_0 = 1.0$. The figure reveals a significant counter-intuitive feature: as b is increased, $A(.5)$ saturates and then even decreases over a wide range of z . The saturation can be understood intuitively as follows: as we increase b , the

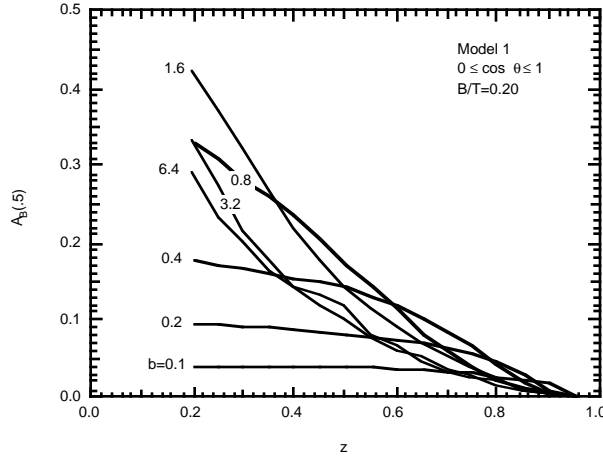


Figure 13: Median B-band extinction $A(.5)$ vs. z for $b=.1, .2, .4, .8, 1.6, 3.2$, and 6.4 .

absorption by dust increases, hence more and more supernovae acquire such large extinctions that they can no longer be observed; (See Fig. 14). The remaining supernovae, which can be observed, are fewer and fewer in number, but they have roughly constant median extinction at given z for sufficiently large b . The slight *decrease* in $A(.5)$ as b increases in a certain range is a more subtle

effect arising because the scale height of SNe progenitors is greater than that of the dust. It can be illustrated by a simple analytical model for the host galaxy viewed face-on (see Appendix).

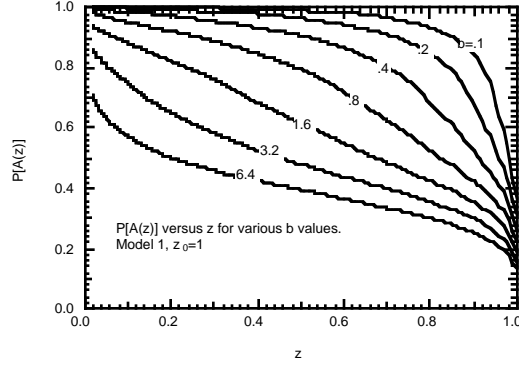


Figure 14: $P[A_0(z)]$, where $A_0(z)$ is the critical extinction at z , for the conditions of Fig. 13.

It is instructive to carry out the following Monte Carlo calculation, which also illustrates the cutoff effect. We choose z at random between $z=0$ and $z = z_0 = 1$ according to the distribution function given by eq.(8), and calculate A_B using Model 1. If $A_B \leq A_0 = 2.5 \ln(1/z)$ from eq. 22, we save A_B and the corresponding z ; otherwise we reject the pair and repeat the calculation. The results are shown in Figs 15,16,17, and 18. In Fig.15 we plot $\langle A_B \rangle$ versus b_0 for the 3 cases: $b = b_0, b = b_0(1+z)^2, b = b_0(1+z)^4$. Here, one can see how $\langle A_B \rangle$ saturates as b_0 increases. In Figs. 16, 17, 18, we plot A_B vs. z for

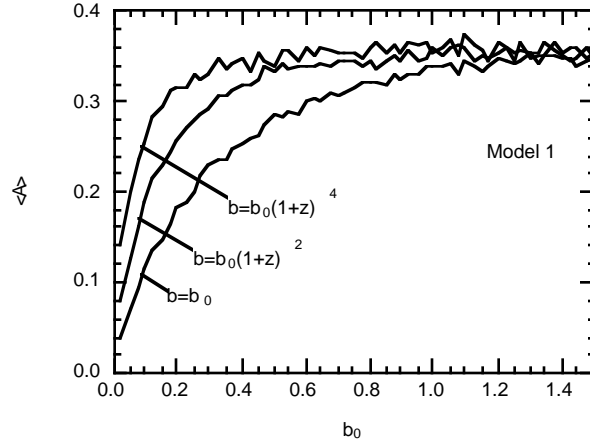


Figure 15: $\langle A_B \rangle$ versus b_0 for the 3 cases: $b = b_0, b = b_0(1+z)^2, b = b_0(1+z)^4$ respectively, with $b_0 = 0.1$. Each of Figs

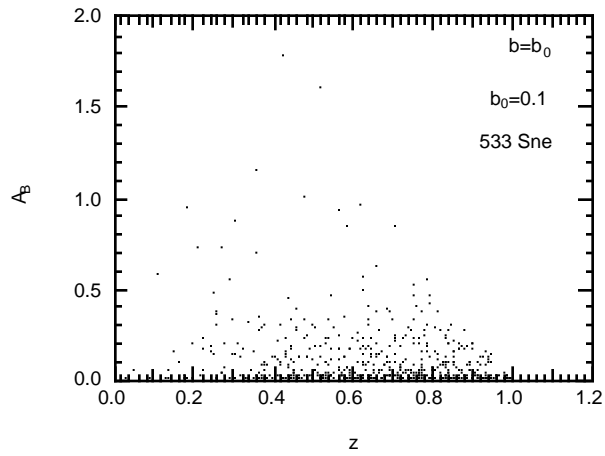


Figure 16: Results of Monte Carlo calculation described in text. $\langle z \rangle = .65$, $\langle A_B \rangle = .11$. Compare this and the next two figures to Fig.3.

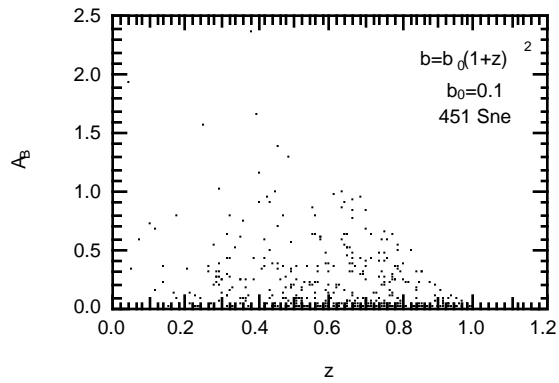


Figure 17: $\langle z \rangle = .62$, $\langle A_B \rangle = .20$, $\langle b \rangle = .27$

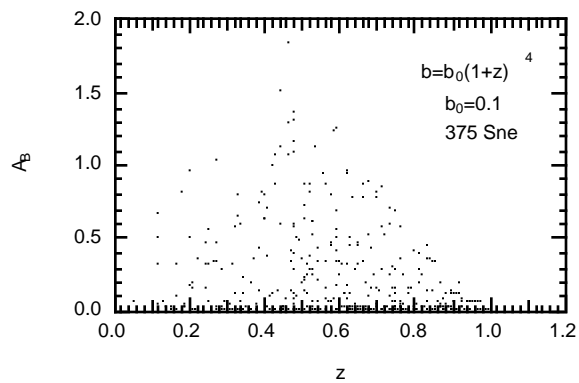


Figure 18: $\langle z \rangle = .61$, $\langle A_B \rangle = .23$, $\langle b \rangle = .74$

16, 17, 18 is qualitatively similar to Fig. 3, despite the very wide range of b values in these calculations.

4 Comparison with observations of Sne Ia in late-type hosts.

4.1 Magnitude-redshift relation. Supernova data

We have selected 16 low- z Sne (Hamuy96, Riess99, Phillips99, Ivanov00) and 29 high- z Sne (Perlmutter99, Sullivan03, Knop03) for comparison with spiral galaxy dust models 1 and 2. All 45 are known (or suspected) to be in late-type host galaxies. To analyze these Sne we assume the magnitude-redshift relation:

$$m_B = M + 5\log_{10}D(z, \Omega_m, \Omega_\Lambda) - \alpha(s - 1) \quad (23)$$

Here, m_B is the peak rest frame B-band apparent magnitude,

$$M = M_B + 5\log_{10}[H_0^{-1}(10pc)^{-1}] \quad (24)$$

where M_B is the peak rest-frame B-band absolute magnitude, H_0 is the Hubble constant in $km\,s^{-1}Mpc^{-1}$, and

$$D(z, \Omega_m, \Omega_\Lambda) = \left[c(1+z) \int_0^z \frac{dx}{\sqrt{(1+\Omega_m x)(1+x)^2 - x(2+x)\Omega_\Lambda}} \right] \quad (25)$$

Also $c = 3 \cdot 10^5 km/s$ is the velocity of light, s is the observed stretch, and α is the stretch/luminosity slope. Eq. (25) expresses D in terms of the independent parameters Ω_m and Ω_Λ ; however in all that follows we assume that $\Omega_m + \Omega_\Lambda = 1$.

The data for the 45 Sne, displayed in Table 2, are based on observational results given in Tables 3, 4, and 5 of Knop03. In our Table 2, column 2 is the supernova; column 3 is the observed redshift; column 4 is the observed $m_{i,B}$ (including a correction for Galactic extinction and a K correction) with the observational uncertainty $\sigma_{i,m}$ in parentheses; column 5 is the observed stretch s_i and its uncertainty $\sigma_{i,s}$, column 6 is the covariance between $\sigma_{i,m}$ and $\sigma_{i,s}$; column 7 is the uncertainty in Galactic extinction $\sigma_{i,G}$, and column 8 is the calculated total uncertainty $\sigma_{i,total}$ in $m_{i,B}$:

$$\sigma_{i,total}^2 = \sigma_{i,m}^2 + \alpha^2 \sigma_{i,s}^2 + 2\alpha cov(m_i s_i) + \sigma_{i,G}^2 + \sigma_{int}^2 + \sigma_0^2 \quad (26)$$

where the intrinsic dispersion in Sne Ia absolute magnitude is assumed to be $\sigma_{int} = 0.11$, (Phillips99), and σ_0 is an uncertainty due to peculiar motion of the host galaxy. In paragraphs to follow we describe maximum likelihood calculations which incorporate eq'ns (23-26) and the data of Table 2 with dust models 1 and 2, the predictions of which are dependent on the parameters Ω_m , M , α , and b . From eq. (26) it is evident that $\sigma_{i,total}$ depends on α . In addition σ_0 depends on Ω_m . However, since all 4 parameters are inter-dependent in a fit, $\sigma_{i,total}$ really depends to some extent on all of them. The values shown in column 8,

Table 2 correspond to the best estimates $\Omega_m = .26, \alpha = 1.244, M = -3.557,$ $b=0.2$ for Model 1.

In Table 2, column 9 contains an effective stretch-corrected peak B-band apparent magnitude $m_{i,B}^{eff}$ and its uncertainty: $m_{i,B}^{eff} = m_{i,B} + \alpha(s_i - 1)$ where here, α is a best-fit value of the stretch/luminosity slope from Knop03. The uncertainties listed here differ from those given in Knop03 because we employ $\sigma_{int} = .11$ whereas Knop03 used $\sigma_{int} = .17$. Note that, generally speaking, there is good agreement between the values of $\sigma_{i,total}$ (column 8) and the uncertainties in $m_{i,B}^{eff}$ in column 9.

Column 10 of Table 2 gives E(B-V) and its uncertainty. The E(B-V) values listed for Sne 1-16 were arrived at as follows. Phillips et al (Phillips99) determined E(B-V) for 62 low-z Sne Ia, of which 39 are in spirals (including Sne 1-16 of Table 2) and 23 in spheroidal galaxies. They calculated E(B-V) from a weighted mean of $E(B - V)_{Tail}, E(B - V)_{Max},$ and $0.8E(V - I)_{Max},$ where the subscripts “Tail” and “Max” refer to epochs of each supernova light curve. Their final result for E(B-V) for each supernova (listed in col. 7 of their Table 2) also takes into account a Bayesian “prior”, used to eliminate the inconvenience of negative E(B-V) values. This prior is based on the model of Hatano (Hatano98). Since our goal is to compare observed E(B-V) values with predictions of our extinction model, we have recalculated the E(B-V) values of Phillips without the Bayesian prior. These revised values for Sne 1-16 appear in column 10 of Table 2.

Finally, column 11 of Table 2 contains “cut-off” B-band magnitudes $m_{i,cutoff}.$ We have employed several different methods to incorporate the cut-off effect in our maximum likelihood calculations, and all these methods yield essentially identical results. The numbers in column 11 correspond to one of these methods, to be described below.

Table 2. Data for 16 low-z SNe Ia (nos.1-16) and 29 high-z SNe Ia (nos. 17-45) in late-type hosts (Pierlucci et al., 1999; Sullivan et al., 2003; Knop, 2003).

1	2	3	4	5	6	7	8	9	10	11
Sn name	z	$m_{iB} (a_{i,m})$	s_i	$Cov(a_{i,m}; a_{i,s}) \times 10^{-3}$	$a_{i,G}$	$a_{i,total}$	m_{iB}^{ef}	$E(B-V)$	$m_{i,cutoff}$	f
1. 1990O	.0302	16.176(.027)	1.106(.026)	.16	.040	.147	16.33(.15)	.034(.037)		19.65
2. 1992P	.0263	16.049(.017)	1.061(.027)	.089	.008	.146	16.14(.14)	.075(.032)		19.65
3. 1992ag	.0259	16.264(.024)	1.053(.015)	.12	.040	.150	16.34(.15)	.136(.047)		19.65
4. 1992al	.0141	14.478(.012)	.959(.011)	-.047	.014	.194	14.42(.19)	.007(.030)		19.65
5. 1992aq	.1009	19.304(.022)	.878(.017)	-.152	.005	.115	19.12(.11)	.017(.042)		19.65
6. 1992b c	.0198	15.103(.008)	1.053(.006)	-.025	.009	.159	15.18(.15)	-.019(.030)		19.65
7. 1992bg	.0357	16.655(.044)	1.003(.014)	.114	.074	.156	16.66(.15)	.019(.037)		19.65
8. 1992bh	.0451	17.601(.020)	1.027(.016)	.173	.009	.127	17.64(.12)	.143(.039)		19.65
9. 1992bs	.0634	18.20(.039)	1.038(.016)	.239	.005	.127	18.26(.12)	.128(.052)		19.65
10. 1993B	.0707	18.37(.044)	1.021(.019)	-.139	.032	.128	18.40(.12)	.154(.038)		19.65
11. 1994S	.0161	14.78(.018)	1.033(.026)	-.269	.007	.179	14.83(.18)	-.003(.036)		19.65
12. 1995ac	.0488	17.049(.011)	1.083(.012)	-.02	.017	.123	17.17(.12)	.109(.054)		19.65
13. 1995b d	.0158	15.316(.009)	1.038(.008)	-.05	.198	.267	15.37(.27)	.242(.074)		19.65
14. 1996C	.0301	16.567(.039)	1.120(.020)	.428	.006	.145	16.74(.14)	.106(.035)		19.65
15. 1996bl	.0348	16.664(.011)	1.031(.015)	-.038	.040	.136	16.71(.14)	.100(.038)		19.65
16. 1996b o	.0163	15.85(.008)	.862(.006)	-.024	.031	.179	15.65(.18)	.340(.035)		19.65
17. 1995ar	.465	23.485(.082)	.909(.104)	-4.344	.006	.158	23.35(.18)	.448(.242)		24.35
18. 1995as	.498	23.686(.066)	1.035(.090)	.548	.005	.175	23.74(.19)	.051(.212)		24.36
19. 1995a y	.480	23.073(.042)	.880(.064)	-1.348	.029	.133	22.90(.14)	.047(.170)		23.90
20. 1995az	.450	22.699(.069)	.973(.064)	-1.424	.047	.148	22.66(.15)	-.089(.144)		23.13
21. 1996cf	.570	23.31(.031)	.996(.045)	-.269	.010	.125	23.30(.12)	-.054(.107)		24.80
22. 1996cg	.490	23.089(.028)	1.011(.040)	-.149	.009	.123	23.11(.12)	.205(.107)		24.56
23. 1996cl	.495	22.829(.024)	.964(.040)	-.07	.007	.123	22.78(.12)	-.033(.075)		24.52
24. 1996cm	.450	23.263(.069)	.899(.061)	-2.687	.012	.127	23.11(.12)	.124(.185)		24.80
25. 1996cn	.430	23.252(.031)	.890(.066)	-.524	.006	.136	23.09(.14)	.332(.097)		24.79
26. 1997F	.580	23.512(.061)	1.041(.066)	-1.392	.010	.139	23.57(.15)	.063(.232)		23.95
27. 1997I	.172	20.339(.014)	.967(.009)	-.024	.013	.113	20.29(.11)	.026(.064)		24.80
28. 1997N	.180	20.377(.019)	1.067(.015)	-.192	.008	.112	20.48(.11)	-.200(.123)		24.80
29. 1997P	.472	23.158(.041)	.888(.039)	-.494	.009	.123	22.99(.12)	-.052(.219)		24.84
30. 1997R	.657	23.885(.052)	.940(.059)	-1.554	.007	.128	23.80(.14)	.032(.222)		24.93
31. 1997af	.579	23.599(.072)	.850(.045)	-2.003	.007	.125	23.38(.12)	-.215(.265)		25.94
32. 1997a j	.581	23.236(.065)	.947(.045)	-1.693	.008	.124	23.16(.12)	-.213(.193)		26.12
33. 1997am	.416	22.582(.076)	1.032(.060)	-2.857	.009	.128	22.63(.12)	-.008(.119)		25.28
34. 1997ap	.830	24.346(.074)	1.023(.045)	-2.161	.005	.124	24.38(.12)	.155(.118)		24.80
35. 1997ek	.863	24.509(.033)	1.056(.058)	.032	.008	.136	24.59(.14)	-.091(.075)		24.80
36. 1997eq	.538	23.208(.023)	.960(.027)	-.031	.011	.118	23.15(.12)	.035(.034)		24.80
37. 1997ez	.778	24.294(.033)	1.078(.030)	.444	.005	.126	24.41(.12)	.095(.068)		24.80
38. 1998as	.355	22.724(.028)	.956(.012)	-.101	.009	.114	22.66(.11)	.158(.030)		24.80
39. 1998a w	.440	23.222(.020)	1.026(.019)	-.199	.007	.113	23.26(.11)	.259(.026)		24.80
40. 1998ax	.497	23.248(.047)	1.150(.032)	-1.125	.009	.115	23.47(.11)	.113(.044)		24.80
41. 1998a y	.638	23.860(.078)	1.040(.041)	-.048	.009	.140	23.92(.14)	.015(.084)		24.80
42. 1998ba	.430	22.971(.047)	.954(.020)	-.372	.006	.119	22.90(.12)	.040(.038)		24.80
43. 1998b e	.644	23.906(.041)	.816(.028)	-.105	.007	.122	23.64(.12)	.106(.065)		24.80
44. 1998bi	.740	23.922(.024)	.950(.027)	-.28	.005	.115	23.85(.11)	.026(.050)		24.80
45. 2000fr	.543	23.065(.020)	1.064(.011)	-.079	.008	.112	23.16(.11)	-.031(.025)		24.80

4.2 Maximum likelihood calculation. 5 and 4-parameter fits.

We now describe the various analyses we have performed to compare the data of Table 2 with our spiral galaxy extinction models 1 and 2. Consider first the normalized probability density function of the random variables $\vec{x} = (m_{i,B}, s_i, z_i, M)$ where M is assumed to be normally distributed about \bar{M} with standard deviation σ_{int} ,

$$P(\vec{x}, \vec{\theta}) = \begin{cases} \frac{P_0(\vec{x}, \vec{\theta})}{N} & \text{if } m_{i,B} < m_{i,cutoff} \\ 0 & \text{if } m_{i,B} > m_{i,cutoff} \end{cases} \quad (27)$$

where $\vec{\theta}$ is the set of 5 parameters $(\alpha, M, \Omega_m, b, \sigma_{int})$, and N is the normalization constant:

$$N = \int_{-\infty}^{m_{i,cutoff}} P_0(\vec{x}, \vec{\theta}) dm \quad (28)$$

P_0 is the convolution of the dust extinction probability $p(A, b)$ (computed here in b increments of 0.05), with the Gaussian distribution of the remaining random variables:

$$P_0(\vec{x}, \vec{\theta}) = \int_0^{\infty} p(A, b) \frac{1}{\sqrt{2\pi\sigma_{i,total}^2}} \exp\left(-\frac{(m_{i,B} - A - \mu_i)^2}{2\sigma_{i,total}^2}\right) dA, \quad (29)$$

and where μ_i is the expectation value of $m_{i,B}$ in the absence of any extinction by dust. In eqs.(27,28) we make use of empirically estimated values of $m_{i,cutoff}$ for those high redshift supernovae for which these values are available. These $m_{i,cutoff}$, supplied to us by G. Aldering, were estimated from telescope and detector sensitivities and from measured seeing. The remaining $m_{i,cutoff}$ are chosen from inspection of the redshift-magnitude diagram. All these values are listed in column 11, Table 2. In fact we have found that the final results of our calculations are quite insensitive to changes in the $m_{i,cutoff}$.

For the set of 45 supernovae the full 5-parameter likelihood function is defined as:

$$L_5(\vec{\theta}) = \prod_{i=1}^{45} P(\vec{x}, \vec{\theta}) \quad (30)$$

L_5 provides the basis for our statistical model; from it we can calculate maximum likelihood estimators (MLE's) under a variety of assumptions. For example, we can calculate the MLE's for all 5 parameters simultaneously. However, as we have mentioned, independent evidence exists that $\sigma_{int} = 0.11$, (Phillips99). Making this assumption, we have a likelihood function L_4 that depends on only 4 parameters.

The results for L_4 are summarized in Table 3. In that Table, columns 3,4, and 5 refer to Models 1 and 2, $\sigma_{int} = 0.11$, and Model 1, $\sigma_{int} = 0.24$, respectively. The last column is included because we wished to test the hypothesis that $\sigma_{int} = 0.11$ by carrying out the full 5-parameter fit. This yielded the surprising result that L_5 reaches maximum for $\sigma_{int} = 0.24$, $b=0$. The probable

explanation for this result is that in making a 5-parameter fit we were attempting to account for the data spread by simultaneously fitting b and σ_{int} ; yet these two sources of variance differ in their third moments (skewness). Thus the 5-parameter fit is actually fitting skewness.

The probability distributions for non-zero values of b have skewness larger than the observed data by at least a factor of 4. Therefore L_5 minimizes skewness by favoring $b=0$. However, skewness is notoriously difficult to measure and model. We do not believe that our dust models are refined enough to predict skewness, and thus we conclude that L_5 gives spurious MLE's. This conclusion is supported by goodness-of-fit statistics which indicate that the $\sigma_{int} = 0.11$ model fits the data better than the $\sigma_{int} = 0.24$ model (see Table 3, section 4).

In Table 3, section 1 gives MLE's of b, Ω_m, M, α from the 4-parameter fit. We then integrate over M, α to find the dependence of the marginal likelihood function on the remaining parameters b, Ω_m . The resulting MLE for b and Ω_m are given in section 2 of Table 3. We next integrate over Ω_m and once again find best estimates as well as confidence intervals for b . These are shown in section 3 of Table 3. Finally we perform a goodness-of-fit analysis (section 4 of Table 3). Here we list the probability P that L_4 generated from the data of Table 2 is greater than an L_4 generated from random data. It can be shown that these probabilities correspond to the values listed for χ^2 with 41 degrees of freedom.

		Model 1	Model 2	Model 1	
		$\sigma_{int} = .11$	$\sigma_{int} = .11$	$\sigma_{int} = .24$	
1.	MLE, 4 param. fit	b	0.2	0.04	0.0
		Ω_m	0.26	0.25	0.28
		M	-3.557	-3.549	-3.349
		α	1.245	1.162	1.380
2.	MLE, 2 param. fit	b	0.2	0.05	0.0
		Ω_m	.26	.26	.28
3.	MLE, 1 param. fit conf. intervals	b	0.2	0.05	0.0
		68%	.14-.28	.00-.09	0-.10
		90%	.11-.36	.00-.11	.00-.11
		95%	.10-.40	.00-.20	.00-.20
		99%	.00-.55	.00-.99	.00-.30
4.	P $\chi^2(41)$.634	.463	.331
			37.3	41.2	44.4

Figs.19-21 show contour plots of confidence regions for the 2-parameter marginal likelihood function in the Ω_m, b plane.

4.3 One parameter fit with the $m_{i,B}^{eff}$. Use of E(B-V) data

In a simpler alternative procedure, we fix Ω_m, M , and α at their best-fit values as determined in (Knop03): $\Omega_m = 0.25, M = -3.48, \alpha = 1.47$, and maximize the likelihood function by varying b . This function is here defined as

$$L_1(b) = \prod_{i=1}^{45} \int_0^{A_{0i}} \frac{1}{\sqrt{2\pi\sigma_i^2}} \exp\left[-\frac{[m'_B - m_{i,B}^{eff} + A]^2}{2\sigma_i^2}\right] p_{i,N}(A, b) dA \quad (31)$$

where $m'_B = m_B + \alpha(s-1)$ from eq. (23), the $m_{i,B}^{eff}$ are from column 9 of Table 2, and the σ_i are their associated uncertainties. Also the $p_{i,N}$ are normalized

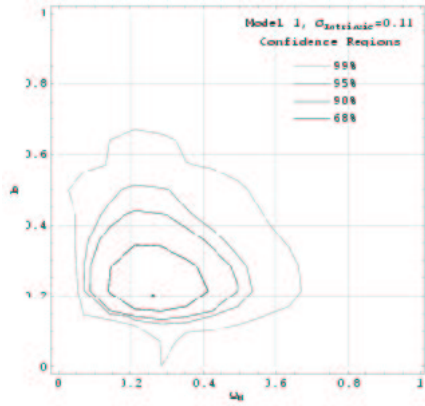


Figure 19: Contour plot for Model 1, $\sigma_{int} = 0.11$

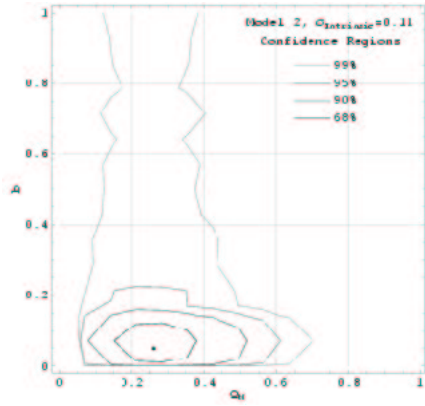


Figure 20: Contour plot for Model 2, $\sigma_{int} = 0.11$

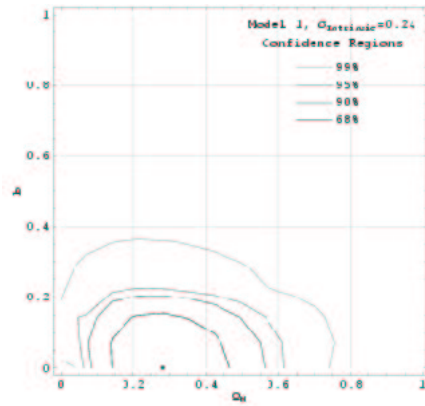


Figure 21: Contour plot for Model 1, $\sigma_{int} = 0.24$

extinction probability distributions:

$$p_{i,N}(A, b) = \frac{p_i(A, b)}{\int_0^{A_{0i}} p_i(A, b) dA}, \quad i = 1, \dots, 45 \quad (32)$$

calculated from either of our dust models, and each distribution depends on z_i because it is cut off at $A = A_{0i}$, and vanishes for all $A > A_{0i}$. Here we express the A_{0i} by means of eq. (21) in terms of limiting redshifts $z_0 = 0.15$ for Sne 1-16, and $z_0 = 1.0$ for Sne 17-45. In this analysis, the increment in b in computation of the $p_{i,N}(A, b)$ was 0.01, and we assume that $\sigma_{int} = 0.11$.

The results are shown in Table 4, section (1). It can be seen that the MLE's for b are very close to those obtained with the 4 parameter fit (see Table 3). Note also that very similar values are obtained if the limiting redshift of Sne 17-45 is chosen as $z_0 = 1.5$ rather than 1.0.

Table 4, section (2) gives results for the supernovae 1-32 of Table 2, (thus excluding the 13 Sne with the highest redshift). This calculation was done to see if there is any evidence for an increase of b with redshift. We find no such evidence; on the contrary, as the results in Table 4 show, b may be very slightly larger for the sample of Sne 1-32 than it is for Sne 1-45.

In Table 4, sections (3), (4), and (5) we show results for various non-standard choices of white dwarf progenitor scale heights, radial scale factors, and B/T values, respectively.

It is also of some interest to employ the E(B-V) values of Table 2, column 10 to construct a likelihood function L_{EBV} with b once again as the sole free parameter, Ω_m , M , and α being fixed as before. We assume $R_V = 3.1$ and thus define a B-band extinction $A_i = 4.29E(B - V)_i$, and a corresponding uncertainty σ_i which is 4.29 times the uncertainty in $E(B - V)_i$. Then we define the likelihood function:

$$L_{EBV}(b) = \prod_{i=1}^{45} \int_0^{A_{0i}} \frac{1}{\sqrt{2\pi\sigma_i^2}} \exp\left[-\frac{[A - A_i]^2}{2\sigma_i^2}\right] p_{i,N}(A, b) dA \quad (33)$$

The results of this calculation are shown in Table 4, section (6). The uncertainties in the MLE's of b obtained here are relatively large, but they are consistent with the values of Table 4, section (1).

Table 4. Results of One Parameter fits.

Condition	Model	Parameters	b at $L_{1,max}$	68% C.I.	95% C.I.
(1) Sne 1-45	1	Standard [†]	.16	.10-.23	.06-.34
	2	Standard [†]	.06	.04-.09	.03-.17
(2) Sne 1-32	1	Standard [†]	.18	.15-.30	.10-.45
	2	Standard [†]	.08	.05-.14	.04-.58
(3) Vary progenitor scale height	1	$h_z = .1kpc$.08	.05-.11	.03-.16
	1	$h_z = .3kpc$.13	.08-.19	.05-.27
	1	$h_z = .7kpc$.18	.11-.25	.07-.35
	2	$h_z = .1kpc$.04	.03-.06	.01-.09
	2	$h_z = .3kpc$.06	.04-.08	.02-.17
	2	$h_z = .7kpc$.07	.05-.09	.03-.22
(4) Vary h_1	2	$h_1 = 0.5kpc$.03	.02-.05	.01-.07
	2	$h_1 = 5.0kpc$.08	.07-.37	.03-.47
(5) Vary B/T	1	B/T=0.0	.17	.10-.22	.06-.32
	1	B/T=.50	.18	.10-.25	.04-.38
	2	B/T=0.0	.06	.05-.12	.03-.21
	2	B/T=.50	.05	.03-.07	.02-.10
(6) E(B-V)	1	Standard [†]	.30	.15-.75	—
	2	Standard [†]	.19	.08-.40	—

[†] Standard: All scale factors for stars and dust as specified in Secs. 3.2-3.4; B/T=.20; $\cos\theta$ uniform and random between 0 and 1.

To summarize our analysis of the 45 supernovae in late type hosts, all of our efforts to compare the data of Table 2 with the spiral galaxy extinction models 1,2 yield essentially the same conclusion: this sample of supernovae is characterized by a small value of the parameter b: $b \approx 0.05 - 0.3$. A priori, we would have expected $b \approx 1$ on the basis of the Drimmel-Spergel model of our Galaxy.

5 Spheroidal hosts

5.1 Spheroidal model

Spheroidal galaxies, like bulges in spiral galaxies, are not spherically symmetric and are frequently even triaxial, but it is a reasonable first approximation for the purpose of modeling to assume spherical symmetry. Usually, the surface brightness distribution can then be approximated by the deVaucouleurs law (eq. 9), and it is an adequate approximation to describe the underlying stellar distribution by a simple function such as:

$$\rho(r) = \frac{\rho_0}{\left(1 + \frac{r^2}{c^2}\right)^{3/2}} \quad (34)$$

where ρ_0 is the central density, while the constant c sets the radial scale and is typically 0.1 to 1 kpc. This expression has the same form as eq. (11). The outer radius R_0 of the galaxy can be chosen to fix the total galaxy mass, and is

typically 100 kpc.

We can obtain some idea of the dust content in spheroidal galaxies by considering the median values of far-infra-red brightness, far infra-red luminosity, and hydrogen gas mass (Roberts94). These numbers suggest that the median dust mass for E/S0 galaxies is roughly 10^6 solar masses, approximately 10% or less of that in early spirals.

Another significant clue comes from observed color gradients in elliptical galaxies. Traditionally these have been attributed to variation in stellar population with respect to radial distance from the galaxy center. However Wise and Silva (Wise96) suggest that dust may play an important, and perhaps dominant, role in establishing the color gradients. They have carried out a radiative transport calculation, including the effects of scattering, and find the best fit to observed color gradients in a sample of 52 elliptical galaxies by assuming a dust distribution of the form: $(r^2 + d^2)^{-1/2}$ with $d \approx .1 - 1 \text{ kpc}$ (spherical symmetry assumed), a large-r cutoff $R=10$ to 30 kpc, and the central dust density fixed to yield, once again, a total dust mass of approximately 10^6 solar masses.

Fig. 22 shows the results of a Monte Carlo calculation with $R=20$, $c=1.0$, $d=1.0$ (all in kpc) and $M_{dust} = 10^6 M_{\odot}$. We plot a histogram of the probability $p(A)$ to find a supernova with extinction between A and $A+.005$, versus A . In the present case, because the total dust mass is an order of magnitude less than in a spiral galaxy, and also because it is now more extended spatially, the extinction is far smaller. For the results shown in Fig.22, the median B-band extinction is $A(.5)=.051$ and the 80'th percentile extinction is $A(.80)=.077$.

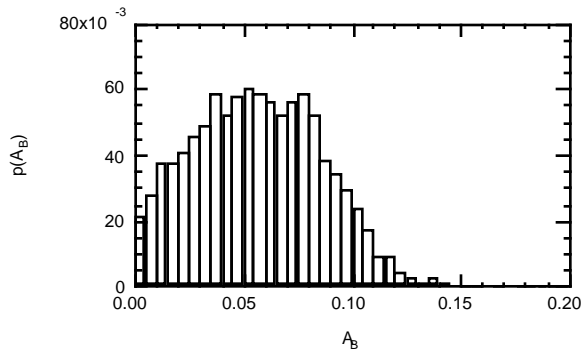


Figure 22: Histogram of the probability $p(A_B)$ to find a supernova with extinction between A_B and $A_B + .005$, plotted versus A_B , for the spheroidal galaxy dust model described in the text.

5.2 Comparison with observed Sne IA in spheroidal hosts

Sullivan et al(Sullivan03) classified 10 high-z Sne Ia in spheroidal hosts. E(B-V) values are known for 8 of these: all are consistent with zero, as is their weighted mean. In the spheroidal model, it turns out that any dust mass from 0 to $5 \cdot 10^6 M_{\odot}$ is consistent with these results. Hence we can make no useful

constraint on the dust mass from these data.

An analysis of $E(B-V)$ for 23 low- z Sne Ia in spheroidal hosts (Ivanov 2000) yields a reasonably good fit with the spheroidal model, assuming $M_{dust} = 2 \cdot 10^6 M_{\odot}$, R_V in the range 2 to 3.1, and a dust outer radius $R=10$ kpc. In view of the large uncertainties in the data and in the model assumptions, we consider these results reasonable. On the other hand, they provide no useful constraints.

6 Summary and Conclusions

Approximately 75% of observed SneIa are found in early and late spiral and irregular hosts, and the bulk of our efforts in this paper have been devoted to understanding the extinctions of these supernovae. In view of present limitations and uncertainties of data on supernovae and galaxies at low and high z , it would be inappropriate to draw very detailed and specific conclusions from the analyses we have presented. Obviously, one cannot take any particular Monte Carlo model (such as our Models 1 and 2) very seriously; they can only serve as rough suggestive guides. Nevertheless, we believe that the following main conclusions are valid:

- (1) One simple and convenient parameter b emerges as central in characterizing the effects of extinction.
- (2) The data we have analyzed favor small values of of this parameter: $b \approx .05 - .25$.
- (3) There is no evidence from these data for an increase of b with redshift z .

Therefore, on the basis of these data we conclude that extinction of Type Ia supernova light due to dust in late-type galaxies does not cause serious systematic error in the determination of dark energy parameters, at the present level of precision. Obviously, however, the data sample of 16 low-redshift Sne and 29 high redshift Sne from late-type hosts utilized here is very limited. We look forward to applying the methods described in this paper to new and precise observations of Type Ia supernovae, as these become available.

7 Acknowledgements

We thank A. Kim, S. Deustua, C. Pennypacker, and P. Stark for useful and interesting discussions.

References

- [Aguirre(99a)] Aguirre A.:1999 ApJ 512,L19
- [Aguirre(99b)] Aguirre A.:1999 ApJ 525, 583
- [Aguirre(00)] Aguirre A.,Haiman Z.:2000 ApJ 532, 28
- [Bacon(60)] Bacon R.:1960 J Appl Phys 31, 283
- [Binney(98)] Binney J., Merrifield M.:1998 *Galactic Astronomy* Princeton, New Jersey; Princeton Univ. Press
- [Brinchmann(98)] Brinchmann J. et al: 1998 ApJ 545, L1
- [Cardelli(89)] Cardelli J.A., Clayton G.C., Mathis, J.S.:1989 ApJ 345, 245
- [Carroll(92)] Carroll S.M., Press W.H.,& Turner E.L.: 1992 Annu Rev Astron Astrophys 30,499
- [Dalcanton(02)] Dalcanton J.J.& Bernstein R.A.: 2002 AA124, 1328
- [Davis(51)] Davis L., Grenstein J.L.:1951 ApJ 114, 206
- [deBernardis(02)] deBernardis P. et al: 2002 ApJ 564, 559
- [deVaucouleurs(48)] deVaucouleurs G.:1948 Ann Astrophys 11, 247
- [Donn(63)] Donn B., Sears G.W.:1963 Nature 140, 1208
- [Draine(84)] Draine B.T., Lee H.M.:1984 ApJ 285, 89
- [Draine(96)] Draine B.T., Weingartner J.C.:1996 ApJ 470, 551
- [Draine(97)] Draine B.T., Weingartner J.C.:1997 ApJ 480, 633
- [Draine(03)] Draine B.T.:2003 Annu Rev Astron Astrophys 41, 241
- [Draine(03a)] Draine B.T.: in *The Cold Universe* ed. Pfenniger D. Berlin: Springer-Verlag in press (astro-ph/0304488)
- [Drimmel(01)] Drimmel R.& Spergel D.: 2001 ApJ 556, 181
- [Falco(99)] Falco E.E. et al:1999 ApJ523, 617
- [Fitzpatrick(99)] Fitzpatrick E.L.:1999 PASP 111, 63
- [Frank(49)] Frank F.C.:1949 Dis Faraday Soc 5, 48
- [Genzel(00)] Genzel R., Cesarsky C.J.:2000 Annu Rev Astron Astrophys 38, 761
- [Hall(49)] Hall J.S.:1949 Science 109, 166

- [Hatano(98)] Hatano K., Branch D., & Deaton J.: 1998, ApJ 502, 177
- [Hillebrandt(00)] Hillebrandt W., Niemeyer J.C.: 2000 Annu Rev Astron Astrophys 38, 191
- [Hiltner(49)] Hiltner W.A.:1949 Science 109, 165
- [Ivanov(00)] Ivanov V.D., Hamuy M., Pinto P.A.:2000 ApJ 542, 588
- [Jansen(94)] Jansen R.A. et al: 1994 MNRAS 270, 373
- [Keel(01)] Keel W.C., White R.E.: 2001 AJ 121, 1442
- [Kent(85)] Kent S.M.: 1985 ApJS 59, 115
- [Kim(95)] Kim S.H., Martin P.G.:1995 ApJ 444, 293
- [Knapen(91)] Knapen J.H. et al: 1991 AA 241,42
- [Knop(03)] Knop R. et al: 2003, ApJ to be published.
- [Majewski(02)] Majewski S.R.& Siegel M.H.: 2002 ApJ 569,432
- [Masters(03)] Masters K.L., Giovanelli R., Haynes M.P.: 2003 AJ 126,158
- [Mathews(01)] Mathews L.D., Wood K.: 2001 ApJ 548, 150
- [Mathis(77)] Mathis J.S., Ruml W., Nordsieck K.H.:1977 ApJ 217, 425
- [Mathis(90)] Mathis J.S.:1990 Annu Rev Astron Astrophys 28, 37
- [Mortzell(01)] Mortzell E., Gunnarsson C., Goobar A.:2001 ApJ 561, 106
- [Paerels(02)] Paerels F., Petric A., Telis G., Helfand, D.:2002 BAAS 34,3,[97.03]
- [Perlmutter(99)] Perlmutter S. et al: 1999, ApJ 517, 565
- [Phillips(99)] Phillips M.M. et al: 1999 AJ 118, 1766
- [Riess(98)] Riess A. et al: 1998, AJ 116, 1009
- [Riess(01)] Riess A. et al: 2001 ApJ 560, 49
- [Roberts(94)] Roberts M.S., Haynes M.P.:1994 Annu Rev Astron Astrophys 32,115
- [Salpeter(77)] Salpeter E.:1977 Annu Rev Astron Astrophys 15, 267
- [Schlegel(98)] Schlegel D.J., Finkbeiner D.P., Davis M: 1998 ApJ 500, 525
- [Sears(55)] Sears G.W.:1955 J Chem Phys 23, 1630
- [Simien(86)] Simien F, deVaucouleurs G.:1986 ApJ 302, 564

- [Soifer(87)] Soifer B.T., Houck J.R., Neugebauer G.: 1987 *Annu Rev Astron Astrophys* 25, 187
- [Spergel(03)] Spergel D. et al: 2003 *ApJS* 148, 175
- [Sullivan(03)] Sullivan M. et al: 2003 *MNRAS* 340, 1057
- [Tonry(03)] Tonry J. et al: 2003 *ApJ* 594, 1
- [van den Bergh(91)] van den Bergh S., Tammann G.: 1991 *Annu Rev Astron Astrophys* 29, 363
- [van den Bergh(02)] van den Bergh S., Li W., Filippenko A.: 2002 *PASP* 114, 820
- [Weingartner(01)] Weingartner J.C., Draine B.T.:2001 *ApJ* 548, 296
- [Will(99)] Will L.M., Annestad P.:1999 *ApJ* 526,242
- [Willson(00)] Willson L.A.:2000 *Annu Rev Astron Astrophys* 38, 573
- [Windt(02)] Windt D.L.: 2002 *ApJ* 564, L61
- [Wise(96)] Wise M.W., Silva D.R.:1996 *ApJ* 461,155

8 Appendix

In Sec.3.5 we described how observational selection can lead to a saturation of the median extinction $A(.5)$ and even to its decrease as b is increased; (recall equations 19-22 and Fig. 13.) Here we illustrate the possibility of decrease in $A(.5)$ by a simple analytical model. Consider a disk galaxy viewed face-on, with the observer at $z = +\infty$, and at first consider only the z dependence of the dust absorption coefficient α and the distribution $j(z)$ of supernova progenitors; (ignore the dependence of these two quantities on r , the distance from galaxy center in cylindrical polar coordinates). Let

$$\alpha = b_0 \operatorname{sech}^2\left(\frac{z}{z_D}\right) \quad (35)$$

and

$$j(z) = -\frac{dN}{dz} = c \cdot \operatorname{sech}^2\left(\frac{z}{z_s}\right) \quad (36)$$

where c is a constant. The extinction of a supernovae located at z is then:

$$A = 1.086b_0 \int_z^\infty \operatorname{sech}^2\left(\frac{z}{z_D}\right) dz = bz_d [1 - \tanh\left(\frac{z}{z_D}\right)] \quad (37)$$

where $b = 1.086b_0$. Inverting (37) we have:

$$z = z_D \tanh^{-1}\left(1 - \frac{A}{bz_D}\right) \quad (38)$$

Also, (37) implies:

$$dz = -\frac{dA}{b} \cosh^2\left(\frac{z}{z_D}\right) \quad (39)$$

Then, from (36), (38) and (39) we obtain:

$$dN = \left(\frac{c}{b} \frac{\cosh^2\left[\tanh^{-1}\left(1 - \frac{A}{bz_D}\right)\right]}{\cosh^2\left[\frac{z_D}{z_s} \tanh^{-1}\left(1 - \frac{A}{bz_D}\right)\right]} \right) dA \quad (40)$$

The quantity in large parentheses on the right hand side of (40) is the probability distribution $p(A,b)$ for this model. Let us assume that $z_s = 4z_D$, which is fairly close to the ratio of scale heights actually employed in Models 1,2. Also, we make use of the identity:

$$\tanh^{-1} y = \frac{1}{2} \ln \frac{1+y}{1-y}$$

to rewrite (40) as:

$$p(A,b) = \frac{c \cosh^2\left[\frac{1}{2} \ln\left(\frac{2b}{A} - 1\right)\right]}{b \cosh^2\left[\frac{1}{8} \ln\left(\frac{2b}{A} - 1\right)\right]} \quad (41)$$

Note that $p(A,b) \rightarrow \infty$ when $A \rightarrow 0$ or $A \rightarrow 2b$; also $p = \frac{c}{b}$ when $A = b$. In Fig. 23, we plot $p(A,b=1)$ and $p(A,b=8)$ vs. A . Let us assume that observational selection gives us the cutoff $A_0 = 1$, indicated by the vertical line at $A=1$. Then it is easy to calculate the median extinctions of the *cut-off* distribution functions from (41). For $b=1$, we find $A(.5)=.139$, while for $b=8$, we have $A(.5)=.118$. The model is made more realistic by including the r dependence of

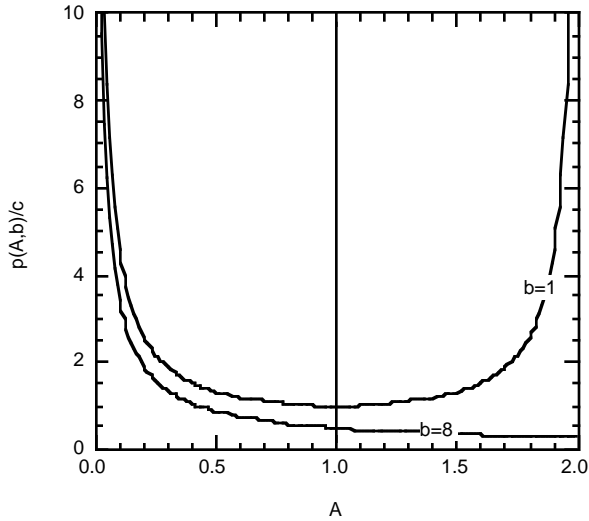


Figure 23: $p(A,b=1)$ and $p(A,b=8)$ vs. A . See eq'n (41).

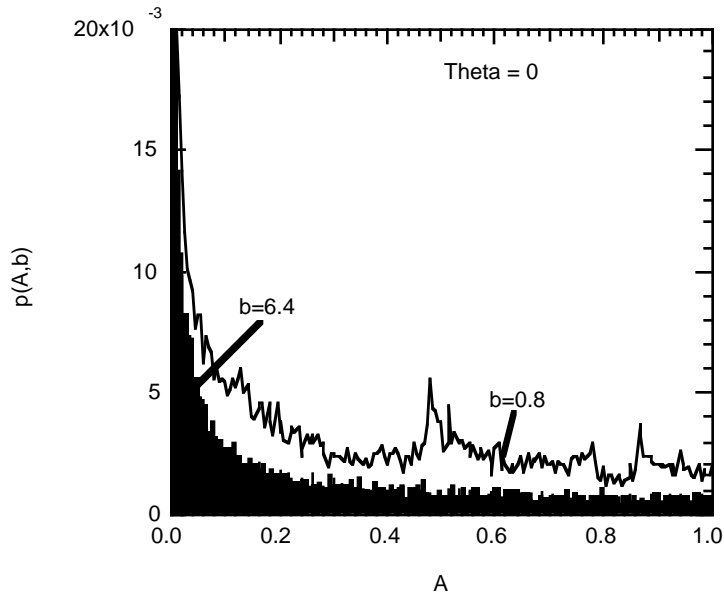


Figure 24: $p(A,b)$ vs. A for Model 1, galaxy face-on; $b=0.8$ and $b=6.4$. Note the peak in $p(A,b=0.8)$ that occurs at $A \approx 0.5$. The median values of A for these two distributions cut off at $A=1$ are $A(.5)=.14$ for $b=.8$, $A(.5)=.05$ for $b=6.4$.

α and j . Then it can be shown that the singularities in $p(A,b)$ disappear; they are replaced by a sharp but finite peak at $A=0$, and finite secondary maxima at various values of $A > 0$. In fact this can be seen in Fig. 24, which shows the result of a Monte Carlo calculation using Model 1, with $b=0.8$ and $b=6.4$, and $\theta = 0$, (galaxy face-on). One can see clearly a secondary peak for $b=0.8$ at $A \approx 0.5$. The median values of A for the distributions cut off at $A=1$ are: $A(.5)=.14$ for $b=.8$, $A(.5)=.05$ for $b=6.4$.